PASJ: Publ. Astron. Soc. Japan **63**, 625–638, 2011 June 25

Gamma-Ray Burst Polarimeter (GAP) aboard the Small Solar Power Sail Demonstrator IKAROS

Daisuke YONETOKU,[1] Toshio MURAKAMI,[1] Shuichi GUNJI,[2] Tatehiro MIHARA,[3] Tomonori SAKASHITA,[1] Yoshiyuki MORIHARA,[1] Yukihiro KIKUCHI,[1] Takuya TAKAHASHI,[1] Hirofumi FUJIMOTO,[1] Noriyuki TOUKAIRIN,[2] Yoshiki KODAMA,[1] Shin KUBO,[4] and IKAROS Demonstration Team

[1]*Department of Physics, Kanazawa University, Kakuma-machi, Kanazawa, Ishikawa 920-1192*
yonetoku@astro.s.kanazawa-u.ac.jp

[2]*Department of Physics, Faculty of Science, Yamagata University, 1-4-12 Koshirakawa-machi, Yamagata, Yamagata 990-8560*

[3]*Cosmic Raditaion Laboratory, RIKEN, 2-1 Hirosawa, Wako, Saitama 351-0198*

[4]*Clear Pulse Co., 6-25-17 Chuo, Ohta-ku, Tokyo 143-0024*

[5] *Institute of Space and Astronautical Science (ISAS), Japan Aerospace Exploration Agency (JAXA), 3-1-1 Yoshinodai, Chuo-ku, Sagamihara 229-8510*

(Received 2010 October 19; accepted 2011 March 3)

Abstract

The small solar-power sail demonstrator "IKAROS" is a Japanese engineering verification spacecraft launched by the H-IIA rocket on 2010 May 21 at Japan Aerospace Exploration Agency (JAXA) Tanegashima Space Center. IKAROS has a 20 m diameter sail, which is made of a thin polyimide membrane. The sail converts the solar radiation-pressure into the propulsion force of IKAROS, and accelerates the spacecraft. The Gamma-Ray Burst Polarimeter (GAP) aboard IKAROS is the first polarimeter specifically designed to measure the polarization of Gamma-Ray Bursts (GRBs) from space, and will do so in the cruising phase of the IKAROS mission. GAP is a modest detector of 3.8 kg in weight and 17 cm in size with an energy range of between 50–300 keV. The GAP detector is now a member of the interplanetary network (IPN) for determining the GRB direction. The detection principle of gamma-ray polarization is the anisotropy of the Compton scattering. Coincidence between the central plastic Compton scattering medium and discrete CsI detectors distributed around the sides of the plastic defines the Compton-scattering angle, which is expected to show an angular dependence if polarization is present in a given GRB. In this paper, we present the GAP detector and its ground-based and onboard calibrations.

Key words: gamma rays: bursts — gamma rays: observations — polarization

1. Introduction

Gamma-Ray Bursts (GRBs) are the most energetic explosions in the universe, and mostly occur at the cosmological distance beyond redshift $z = 1$. The current record for the highest redshift is GRB 090423 at $z \sim 8.2$ (e.g., Tanvir et al. 2009; Salvaterra et al. 2009). In the brightest case, the isotropic luminosity reaches $10^{54}\,\mathrm{erg\,s^{-1}}$. Many physical properties of GRBs have been revealed since the discovery and localization of afterglows by the BeppoSAX mission (Costa et al. 1997). Theoretically, the prompt emission and the following afterglow are thought to be generated by synchrotron radiation in the relativistic jet. The electrons accelerate to almost the speed of light due to relativistic shocks, and a strong magnetic field above 10^4 gauss is generated within the jet in a short time interval of the prompt phase (e.g., Rees & Mészáros 1992; Piran 1999). Many observational and theoretical studies have addressed the physical properties of GRBs, like a jet (e.g., Waxman et al. 1998; Frail et al. 2001), afterglow dynamics (e.g., Panaitescu & Kumar 2001; Nousek et al. 2006), and supernova association (e.g., Galama et al. 1998; Hjorth et al. 2003). However, much more remains to be learned about their emission mechanism which produces gamma-rays.

There are several empirical correlations between the rest-frame physical quantity of GRBs and their luminosity (or isotropic energy $E_{\rm iso}$). The variability–luminosity correlation indicates that the more variable the more luminous (Fenimore & Ramirez-Ruiz 2000). The lag–luminosity correlation is reported by Norris, Marani, and Bonnell (2000) and Schaefer, Deng, and Band (2001). Each pulse in the prompt emission has a time delay of the soft-band emission as compared with the hard-band one. This correlation shows that those events with a large spectral time lag are dimmer than ones with a short lag. These two correlations are based on the temporal behaviors of prompt emission. Several correlations concerning the spectral property have also been suggested. Amati et al. (2002) found a very tight correlation between the spectral peak energy ($E_{\rm p}$) and the isotropic energy ($E_{\rm iso}$) (see also Amati et al. 2006). This $E_{\rm p}$–$E_{\rm iso}$ correlation was confirmed and extended toward X-ray flashes by Sakamoto et al. (2004) and Lamb et al. (2004). Independently, Yonetoku et al. (2004) reported a similar, but tighter correlation between $E_{\rm p}$ and the 1 s peak luminosity ($L_{\rm p}$), called the $E_{\rm p}$–$L_{\rm p}$ correlation. Moreover, using the jet opening half-angle, Ghirlanda, Ghisellini, and Lazzati (2004) found that $E_{\rm p}$ strongly correlates with the collimation-corrected gamma-ray energy (E_γ).

However, the physical reasons for these correlations are not yet established. These empirical properties may indicate that there is well-ordered physics in the complex behaviour of prompt GRBs. Thus, the emission mechanism may play

an important role in these correlations. If the synchrotron radiation in the strong magnetic field is realized on a short time scale of GRB prompt emission, the polarization degree of emitted photons is expected to be very high. Therefore, direct measurements of the polarization degree of the prompt emission is a key to revealing the emission mechanism and the site. As discussed in Lazzati et al. (2004) and Toma et al. (2009), the expected polarization degree, P, is different for various models of the emission mechanism; for example, $P \sim 40\%$ and $P \sim 0\%$ are for synchrotron emission with a well-ordered and random magnetic field, respectively. If we assume a Compton drag model, some fractions of GRBs show $P \sim 80\%$ if the observer is located on the edge of the jet opening angle. The time variations of polarization degree and its angle may tell us the magnetic-field structure on the jet surface and/or in each internal shock.

The first X-ray polarimeter was a Bragg reflection type aboard the OSO-8 satellite in the 1970s (Kestenbaum et al. 1976). This polarimeter worked for monochromatic X-rays of 2.6 keV and 5.2 keV. The first detection of X-ray polarization came from observations of the Crab Nebula (Weisskopf et al. 1976) with $15.7\% \pm 1.5\%$ at 2.6 keV and $18.3\% \pm 4.2\%$ at 5.2 keV. After 30 yr of the first Crab observation, Dean et al. (2008) again measured the polarization of the Crab Nebula as $46\% \pm 10\%$ in the energy range of from 0.1 to 1 MeV of SPI and IBIS aboard the INTEGRAL satellite.

Concerning the GRB polarization, there were earlier reports of the measurement (Coburn & Boggs 2003; McGlynn et al. 2007). Coburn and Boggs (2003) reported a clear detection with a polarization degree of $P = 80\% \pm 20\%$ in GRB 021206 using the RHESSI solar observation satellite. However, reanalyzing the same data, Rutledge and Fox (2004) failed to confirm the results of Coburn and Boggs (2003), and concluded that the polarization of GRB 021206 is consistent with 0%. Wigger et al. (2004) independently checked their analyses, and found a polarization value of $41\%^{+57\%}_{-44\%}$, which is different from the two previous reports, but consistent with all levels of polarization. On the other hand, using INTEGRAL data of GRB 041219A, McGlynn et al. (2007) reported possible detection of polarization with $63\%^{+31\%}_{-30\%}$ for a brightest single pulse, and also $96\%^{+39\%}_{-40\%}$ for a short period including the brightest pulse.

Recently, several types of X-ray and gamma-ray polarimeter have been under development. For the Bragg reflection type, Kitamoto et al. (2010) developed an X-ray polarimeter with a transmission multilayer. They demonstrated that this polarimeter works in the energy band of $\sim$0.1–a few keV. Using the track of the electron ejected by the photoelectric absorption, the polarization of soft X-rays is detected in a gas chamber with imaging capability (Bellazzini et al. 2003; Tanimori et al. 2004; Tamagawa et al. 2006). Based on this technology of the gas imaging polarimeter, the Gravity and Extreme Magnetism SMEX (GEMS) is being developed for a planned launch in 2014 (Swank et al. 2008).

However, the typical energy band of GRBs is 50–300 keV, where the cross section of the Compton scattering dominates that of the photoelectric absorption for light element materials. Therefore, it is more efficient to use the anisotropic angular distribution of the Compton-scattered photons. Several types of polarization detectors utilizing this process are being developed, not only for satellites, but also for balloon experiments. One example is the prototype of the PHENEX instrument by Gunji et al. (1994, 1997, 2007) and Kishimoto et al. (2007). The Polarization Gamma-ray Observer (PoGO) is a honeycomb-shape detector that is composed of a hexagonal well-type scintillator array that utilizes the phoswich technique (Kamae et al. 2008). The octagonal scintillators (Mihara & Miyamoto 2004), and matrix layout using the multianode photomultiplier tubes (Suzuki et al. 2006) are the basis of the PoGO system. These instruments are designed for a narrow field of view to observe steady X-ray and gamma-ray sources, such as the Crab Nebula, pulsars, black-hole candidates, and active galactic nuclei. However, for GRB observations, a wide field of view is required. Yonetoku et al. (2006) showed the basic concept of the GRB polarimeter (GAP) (see also Yonetoku et al. 2006, 2010; Murakami et al. 2010).

In this paper, we shortly introduce the solar power sail satellite "IKAROS", and present ground-based and also in-flight-calibration data to ensure our measurements of polarization of prompt emission of GRBs.

2. Solar Power Sail and Design of GRB Polarimeter

2.1. The Solar Power Sail: IKAROS

The small solar power sail demonstrator "IKAROS" (Kawaguchi et al. 2008; Mori et al. 2009) is a Japanese engineering verification spacecraft launched on 2010 May 21 at Japan Aerospace Exploration Agency (JAXA) Tanegashima Space Center together with the Venus Climate Orbiter AKATSUKI (Planet-C). IKAROS stands for "Interplanetary Kite-craft Accelerated by the Radiation Of the Sun". The weight of the IKAROS spacecraft is 307 kg, and the size is 1.58 m in diameter and 0.95 m in height. IKAROS has an extremely thin, 7.5 μm polyimide membrane with 20 m diameter, as shown in figure 1. Reflecting the photons from the Sun, this sail transmutes solar radiation pressure into propeling power of the spacecraft. This satellite rotates with an angular speed of $\sim$1–2 rotations per minute (rpm) to keep the sail spreading with the centrifugal force. The purpose of this mission is to demonstrate the solar-sail performance in interplanetary space. After the launch, IKAROS successfully deployed the solar sail on 2010 June 9, and started sailing to Venus. The sailing speed of IKAROS can be accelerated or decelerated by changing the inclination angle of $\sim \pm 45^\circ$ against the radiation pressure of the Sun. If IKAROS is accelerated (decelerated), the spacecraft gains (loses) an angular momentum in orbit around the Sun, and it moves toward an outer (inner) orbit. Therefore, we can control the sailing direction of IKAROS and also demonstrate the solar-sail technology even if IKAROS sails in the direction of the inferior planet Venus.

According to the current schedule, IKAROS will pass Venus in half a year after its launch, and go beyond 2 AU from Earth in $\sim$2 yr. During its cruising phase, GAP measures the gamma-ray polarization of the prompt emission of GRBs. Accurate positions of GRBs will be determined by the Interplanetary Network (IPN), of which IKAROS/GAP is a member.

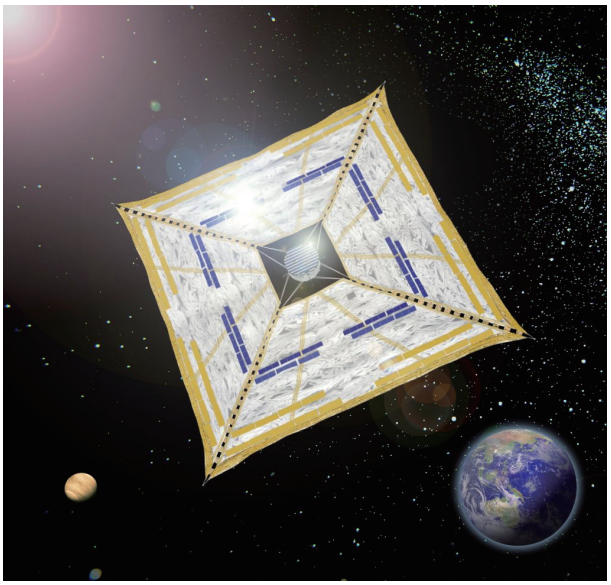

Fig. 1. Schematic view of the IKAROS spacecraft after sail deployment. The GAP detector is mounted at the antisolar side of the spacecraft. Courtesy of JAXA.

In the following sections, we show the design of the gamma-ray polarimeter GAP, with its pre-flight and in-flight calibration data, and numerical studies of *Geant-4* simulations.

2.2. *Gamma-Ray Burst Polarimeter: GAP*

GAP is the "GAmma-ray burst Polarimeter", which consists of two components: the detector unit (GAP-S) and the power-supply unit (GAP-P). GAP-S is a very small detector of 17 cm in diameter and 16 cm in height, as shown in figure 2. A small square box beside GAP-S is GAP-P, which contains two current limiting DC-DC converters to drive the electronics and two high-voltage modules set in GAP-S. GAP-S and GAP-P are 3.69 kg and 0.16 kg in weight, respectively. The total power is ~ 5 W, including both GAP-S and GAP-P. Hereafter, we simply call this system "GAP".

GAP is mounted on the bottom panel of IKAROS, which faces in the antisolar direction. Therefore, GAP always observe the deep universe during the cruising phase of IKAROS. The cylindrical detector cases (chassis), except for the detector top, are covered by thin lead sheets 0.3 mm or 0.5 mm in thickness to reduce the effects of the cosmic X-ray and gamma-ray background, intense soft X-ray transients, and solar-flare events occurring outside of the GAP field of view.

2.3. *Design of GAP*

The polarization detection principle of GAP is the angular anisotropy of the Compton scattering. The cross section of the Compton effect is due to the Klein–Nishina formula,

$$\frac{d\sigma}{d\Omega} = \frac{r_0^2}{2}\frac{E^2}{E_0^2}\left(\frac{E_0}{E} + \frac{E}{E_0} - 2\sin^2\theta\cos^2\phi\right), \tag{1}$$

where r_0 is the classical electron radius. The E_0 and E values are the energies of the incident and the scattered gamma-ray photons, respectively. Here, θ denotes the scattering angle, and ϕ means the azimuth angle measured from the polarization vector (electric field vector) of an incident photon. The relation between E and E_0 is well known as

$$E = \frac{E_0}{1 + \dfrac{E_0}{m_e c^2}(1 - \cos\theta)}. \tag{2}$$

Here, m_e is the electron mass and c is the speed of light in a vacuum. For instance, assuming the nonrelativistic case of $E_0 \ll m_e c^2$ and a scattering direction of $\theta = \pi/2$ plane, the Klein–Nishina formula is approximately described as

$$\frac{d\sigma}{d\Omega} \simeq r_0^2 \sin^2\phi. \tag{3}$$

The amplitude of the modulation is basically proportional to a function of $\sin^2\phi$ in the $\theta = \pi/2$ plane. By detecting the $\sin^2\phi$ modulation from astronomical phenomena, we can measure the degree of linear polarization.

In figure 3, we show the basic concept of our gamma-ray polarimeter GAP. A dodecagon (twelve-sided polygon) plastic scintillator with a single nonposition sensitive photomultiplier tube: PMT (R6041 Hamamatsu Photonics)[1] is attached at the center, and 12 CsI scintillators with PMT (R7400-06 Hamamatsu Photonics)[1] are set around it. The photocathode of R6041 is a super bialkali type, and its electrode structures are designed to withstand strong pyro-shock and vibration during the rocket launch. The central plastic works as a Compton scatterer, and the angular distribution of scattered photons coinciding with the plastic scintillator is measured by the surrounding CsI scintillators each with an angular resolution of 30°. We first considered a multianode PMT to measure the scattering position by the central plastic indicating a high sensitivity to polarization. However, in the developing phase of GAP, the multianode PMTs were known not to survive the strong-shock and random-vibration environments during the rocket launch. Thus, we avoided risk, and took advantage of high geometrical symmetry to reduce fake modulation. All of the PMTs were tested, and reached the vibration levels of pre-flight qualification for JAXA at the Industrial Research Institute of Ishikawa. They also stood the qualification shock test on the 1000 G_{srs} level at Institute of Space and Astronautical Science (ISAS)/JAXA. Here, the shock level in units of G_{srs} is defined as the amplitude of a shock response spectrum within a short time interval of ~ 1 ms.

We first designed 7 cm in depth for the plastic of the pre-flight model (PFM) because it is fully enough one Compton (Thomson) length to scatter photons of 100 keV; however, to reduce the weight of GAP, the depth of the flight model (FM-GAP) was changed to 6 cm. Since the scattered photon should escape from the plastic and reach CsI, it is also important for the radius of the plastic to be shorter than one Thomson length. The CsI scintillators have to stop scattered photons with great efficiency, and thus we determine a thickness of 5 mm, providing stopping powers of almost 100% at 100 keV and $\sim 60\%$ at 200 keV. We cannot avoid multiple-scattering events in the central plastic scintillator because it is read out by the nonposition sensitive PMT. These events reduce the sensitivity

[1] ⟨http://jp.hamamatsu.com/en/index.html⟩.

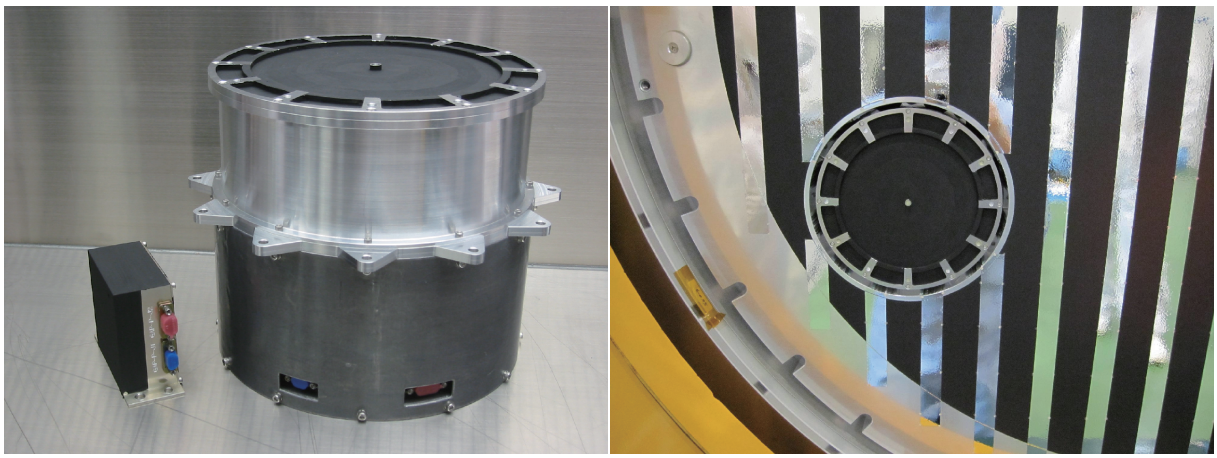

Fig. 2. Left: Photo of GAP-S and its power unit (GAP-P). Right: Photo of GAP installed on the IKAROS spacecraft. A circle in the center of the photo is the top surface of GAP-S. The strips painted in black and silver are the surface of heat radiation into the space and this side faces in the antisolar direction.

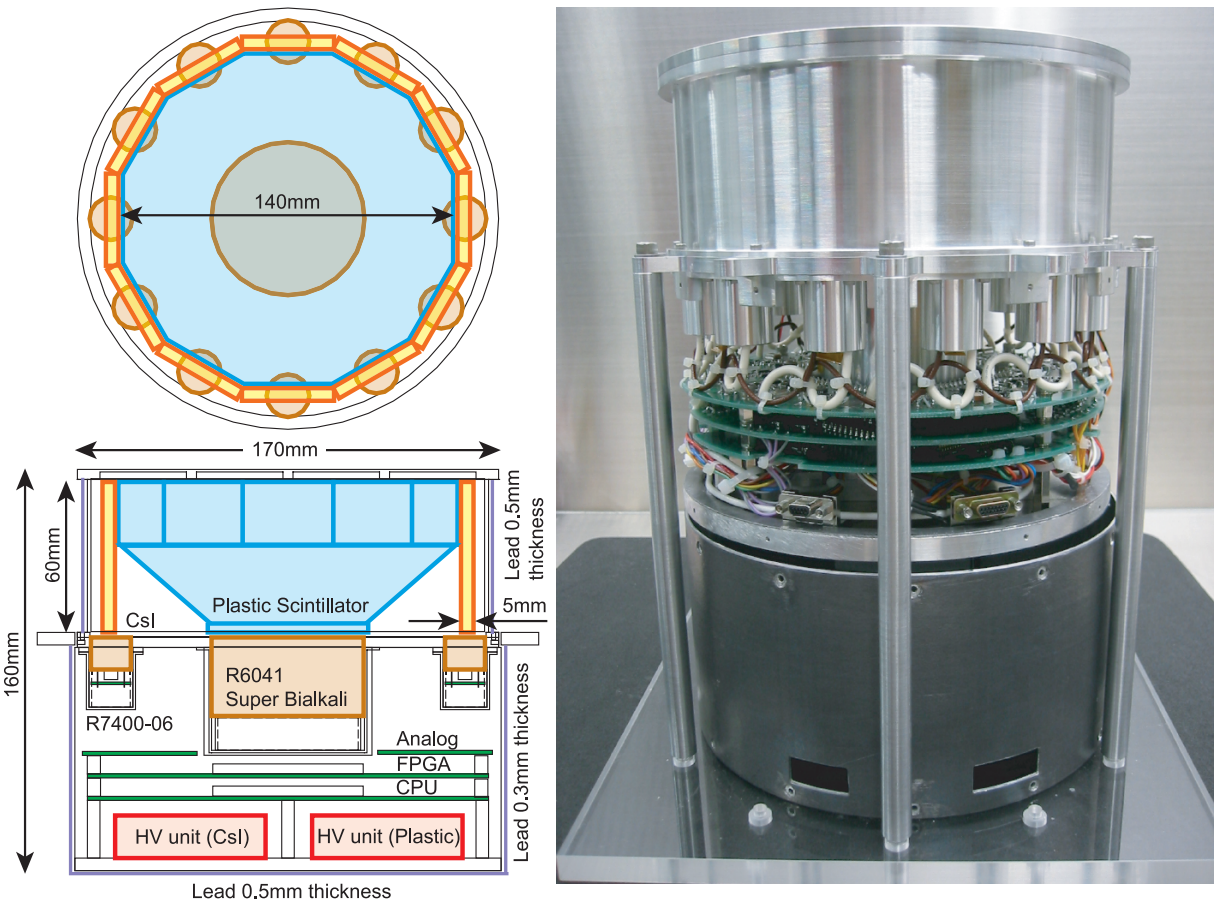

Fig. 3. Left: Schematic view of the GAP sensor. A large plastic scintillator with a super bialkali cathode of PMT (R6041) is attached at the center, and 12 CsI scintillators with small PMTs (R7400-06) are set around it. Right: The photo of GAP whose lead shield is opened.

of the polarization measurement. We consider this point using the Geant-4 simulator in section 4.

2.4. *Brief Summary of Electronics and Data Acquisition System*

GAP has 13 analog outputs (1 plastic and 12 CsI scintillators). In figure 4, we show a flow chart of the readout circuit. These 13 signals are read out by 13 discrete analog electronics arrays. The PMT output is read out through preamplifiers, shaping amplifiers, and discriminators. Once the gamma-ray photon is triggered by any PMT, analog signals of all PMTs are converted to digital signals with an

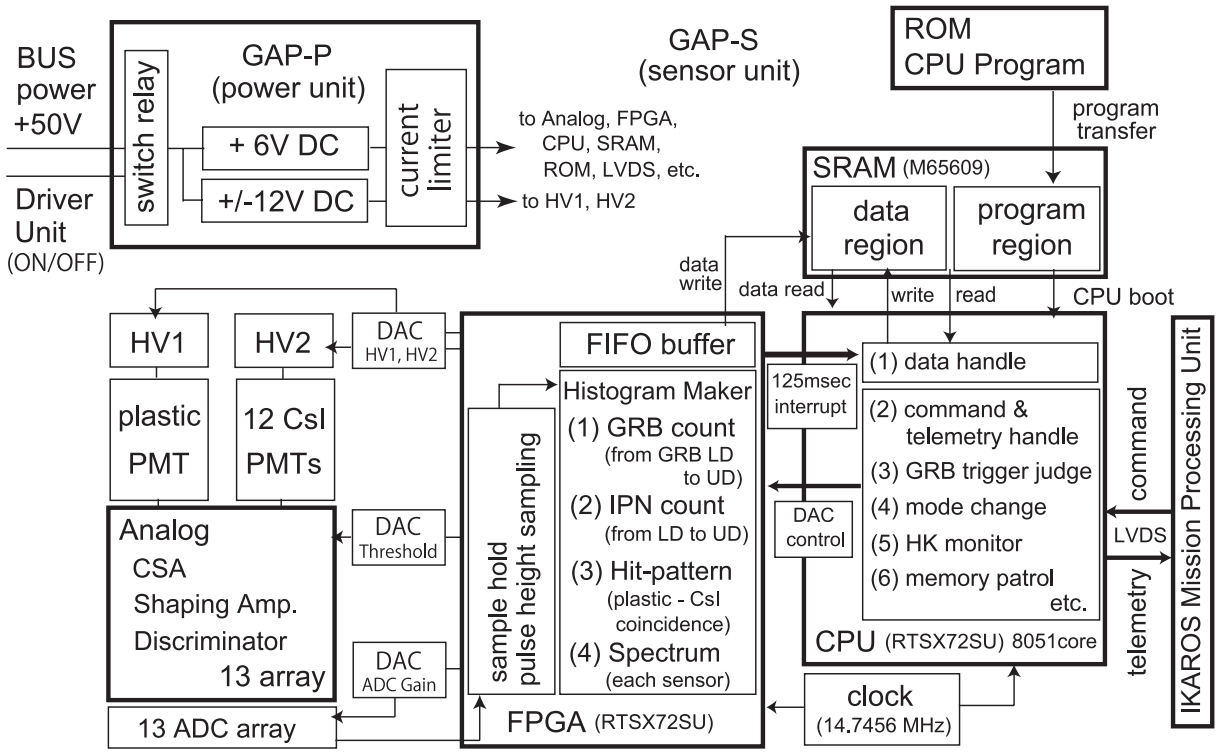

Fig. 4. Flow chart of the readout circuit. The analog outputs from 13 PMTs are read out by 13 discrete analog electronics arrays. Triggered by the output of the discriminator, the FPGA reads the A/D values of all channels. Then, the FPGA analyzes the pulse height, and makes the coincidence within a timing window of 5 μs. The CPU appropriately edits the data every observation mode, and transfers it to the IKAROS mission processing unit and mission data recorder.

analog-to-digital converter, and the following FPGA reads all of their digital values. Then, the FPGA analyzes all pulse heights within a timing window of 5 μs, and selects the plastic–CsI coincidence event as a polarization signal, if there is a plastic signal.

The FPGA integrates the counting rate (light curve), spectra, and hit-pattern of polarization for 125 ms, and creates histogram data. Then, the FPGA interrupts the CPU processing every 125 ms and transfers the data to the CPU. The CPU edits these data according to each observation mode, which is explained in the next section. The edited data by CPU are transferred to the IKAROS Mission Processing Unit (MPU), and are stored as a telemetry packet in the mission data recorder.

The CPU acts as the command and control unit for GAP. It controls several digital-to-analog converters used for the threshold, gain, power level settings, and so forth. We can monitor House Keeping (HK) data, such as the temperature, voltage, current, and simple light curves. We employed a memory patrol system with the majority logic in the CPU, so the single-bit memory error can be repaired by the CPU, itself. This function reduces the probability of CPU hang-up and/or missed operations. GAP used radiation-tolerant and MIL class electronic parts for the core devices, such as FPGA, CPU, SRAM, and LVDS, but not for ROMs. Almost all key devices of the GAP circuit resisted two types of tests, such as ^{60}Co gamma-ray irradiation and 200 MeV of proton irradiation, to select qualified devices at the Tokyo Metropolitan Isotope Research Center and at the Wakasa-Wan Energy Research Center.

When we switch on the GAP power unit, the CPU program stored in ROM is transferred to the program region of the radiation-tolerant SRAM. Then, the CPU starts to work and the ROM device is switched off. The core of CPU is equivalent to an 8051 processor, which is burned in the same FPGA device, RTSX72SU. The observation and HK data are temporarily stored in the data region of SRAM, and are transferred to the IKAROS mission processing unit with the LVDS communication when the CPU receives data request commands. Two high-voltage modules are supplied from Meisei Electric Co., Ltd; these are the same type as those used for the Suzaku and Kaguya satellites of JAXA.

3. Observation Mode

The GAP has a calibration mode and two observation modes (GRB and CRAB). The CRAB observation mode is a standard operating mode, and when a GRB is detected the mode temporarily switches to the GRB mode for 176 s. After that, the next CRAB mode starts by a prescheduled command. At regular intervals during the mission, the calibration mode is used to monitor the gain of detectors.

The onboard CPU continually monitors the gamma-ray count rate every second. If the count rate suddenly increases beyond the preset value, the CPU switches on the GRB mode. The criterion for a GRB trigger is an increase of the count rate in the energy range of from GRB_LD to UD, $\sim$ 220 keV.

Here, the discriminators GRB_LD to UD define the energy range of interest in GRB triggers. The detailed criterion is explained in subsection 3.2. We can set this GRB_LD for each sensor, and the nominal value is ~ 60 keV for 12 CsI scintillators and 20 keV for the plastic one. We set this GRB_LD much higher than the sensor LD of ~ 30 keV for CsI and ~ 8 keV for plastic to avoid noise fluctuations, and also to avoid any intense soft X-ray transient.

3.1. CRAB Mode

The CRAB mode is the standard observing mode that continuously monitors the field of view of GAP. When viewing the anti-Galactic center direction, the Crab pulsar at the Crab Nebula is the brightest source, if the transient A 0535+26 is in quiescence. Using the phase information of IKAROS's rotation period measured with the Sun pulse interval (approximately 1 rpm), GAP can stack the polarization data during the CRAB mode. GAP starts the integration at the time of the Sun pulse in order to determine the phase angle of the polarization vector. Of course, when the count rate significantly increases and the GRB flag is set, the CPU switches to the GRB mode.

According to the current plan of the IKAROS attitude, GAP observes along the ecliptic, which crosses at the Galactic plane near the Galactic center, and also at its opposite direction, very close to the Crab Nebula. There are few bright objects close to the Crab Nebula, and the Crab Nebula is expected to be observed within 15°–20° from the GAP's detector axis from the end of 2010 November to the beginning of December. Thus, we will spend 90% of the observing time in the CRAB mode, and we will try to measure the polarization from the Crab Nebula, since the contributions from individual objects in the GAP 2π anti-Galactic center field of view are not expected to be significantly polarized. When viewing in the direction of the Galactic center, Sco X-1 and other bright X-ray sources will preclude identifying the source of any polarization detected. Therefore, we consider that the Crab Nebula is the only object to enable polarization analyses to be performed.

In this CRAB mode, GAP obtains the spectrum of the plastic scintillator, the summed spectrum of 12 CsI scintillators in 16 Pulse Height Analyzer (PHA) channels, and polarization of 2 energy bands (LD–HITPAT_LH and HITPAT_LH–UD) with an angular resolution of 15° (24 angular bins). The angular resolution is determined by the IKAROS rotation angle, while GAP has only 12 CsI scintillators. The exposure of each CRAB mode can be set in the range of from 30 s to 8.5 hr, and we usually set the CRAB mode to ~ 110 min integrations. This time interval is determined to avoid buffer overflow of the integrated spectra. The CRAB mode starts by the scheduled command every 120 min. The remaining 10 min are used to transfer the data to MPU, and then the GAP-CPU waits for the start command of the next CRAB mode.

We show two spectra in the CRAB mode for the plastic and CsI detectors during the 110 min integration in figure 5. The Crab Nebula, itself, was out of the field of view. If GAP observes the sky without any strong X-ray/gamma-ray sources, these two spectra should be mainly explained by the Cosmic X-ray Background (CXB) and particle-induced background; for example, neutron scattering events, or gamma-rays from the spacecraft body activated by particle. The particle background is rejected by the UD of each scintillator and by the multiple coincidence logic. However, GAP has a wide field of view, and has observed a portion of the Galactic bulge, during the first two months since the GAP switch-on.

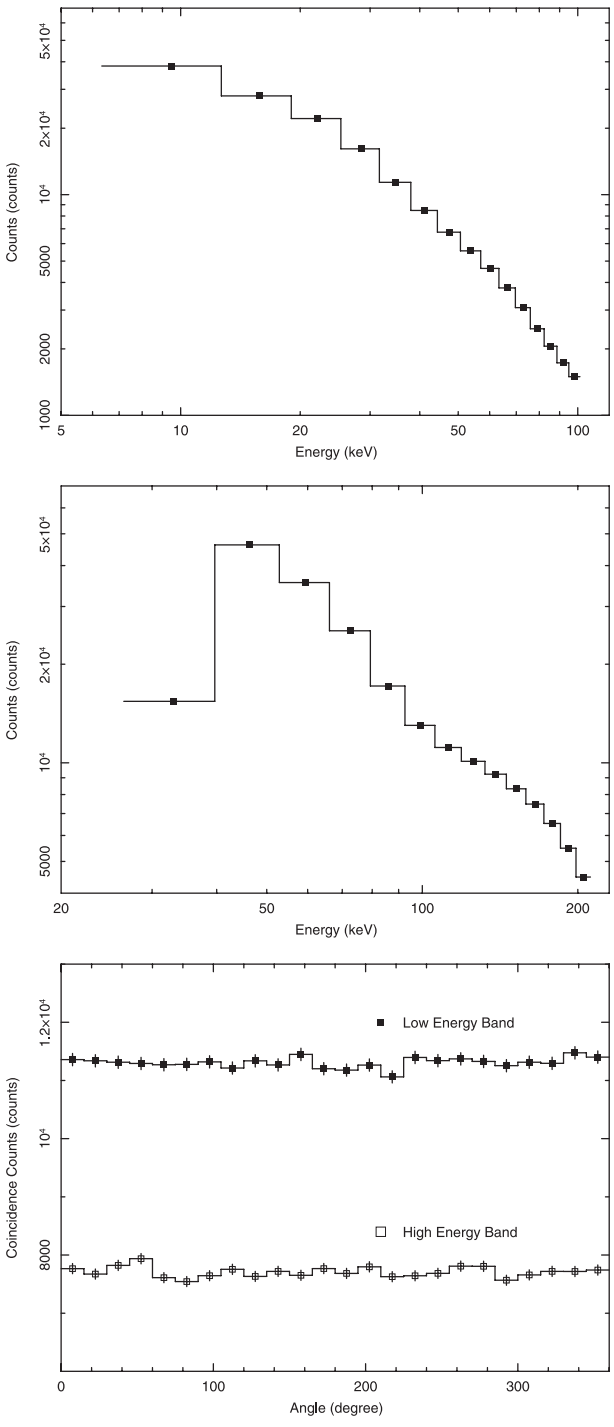

Fig. 5. Data examples of the CRAB mode during a 110 min integration time. The Crab Nebula, itself, was out of the field of view (FOV). Instead, the Galactic center was in the FOV. Therefore, the data are the cosmic X-ray/gamma-ray background and the sources near the Galactic center. Top: The spectrum of the plastic scintillator. Middle: The spectrum of 12 CsI sensors. Bottom: The polarization data of the low-energy (filled square) and high-energy (open square) bands.

Therefore, these two spectra are a mixture of the CXB and some Galactic bulge sources.

As shown in the bottom of figure 5, both modulation curves are flat. When we adopt the constant model, the fitting results of low- and high-energy bands are $(1.130 \pm 0.004) \times 10^4$ with $\chi^2 = 16.0$ for 23 degrees of freedom and $(7.706 \pm 0.030) \times 10^3$ with $\chi^2 = 24.3$ for 23 degrees of freedom, respectively. Here, the error is at the 90% confidence level. The observed modulation is quite flat within the 1% level for long integration of the CXB and Galactic bulge sources in the CRAB mode. This result does not confirm anything quantitative about the ability or sensitivity for GAP to measure polarization, but strongly supports the flatness of the GAP angular response for the nonpolarized background data; also, systematic associations with background are small.

3.2. GRB Mode

The GRB trigger is based upon testing the 1s rate to determine whether it has increased by 8σ when compared with an average counting rate for the last 8 s. The significance of the trigger level is adjustable by the ground command up to 80σ in 256 steps. GAP has a ring buffer memory that stores the last data of 16 s of the coincidence hit-pattern (polarization), and light curve, except for the spectrum. Once the CPU switches on the GRB mode, as shown in table 1, the CPU records 12 polarization data with the coincidence between plastic and each CsI, a summed light curve, and a summed CsI spectrum for 176 s from the time of GRB trigger ($T = 0$). Then, the GAP's ring buffer memory is frozen, and the GAP-CPU also records the data for 16 s ahead of the trigger ($-16 \leq T < 0$). As already mentioned, the timing window of each coincidence is $5\,\mu$s. Therefore, we can ignore any deadtime correction, even if GAP detects the brightest GRBs in the Burst and Transient Source Experiment (BATSE) catalog.

We can also start the GRB mode manually by sending a mode-change command to record the background data in the GRB mode. In figure 6, three panels show the light curve, background spectrum, and polarization (coincidence) data of the GRB mode. We show the GRB light curve with the energy ranging between LD and UD, and it contains the data with two kinds of time resolutions. As summarized in table 1, in the first 32 seconds from the GRB trigger ($0 \leq T < 32$), the light curve is recorded with a high resolution of 125 ms, which is suitable for interplanetary network (IPN) to determine the GRB direction together with other satellites. In the following 144 seconds ($32 \leq T < 176$) and in the 16 seconds ahead of the trigger ($-16 \leq T < 0$), the light curves are recorded with a time resolution of 1 s. At the same time, one integrated spectrum is obtained in the time interval of $0 \leq T < 176$ with 16 PHA channels, as shown in the middle panel. These spectral data contain the photons of 12 CsI scintillators with only a single hit event. The bottom panel shows the summed polarization data of the low- and high-energy bands as a function of the phase angle, ranging from $t = -16$ to $t = 176$ in the manual GRB mode, respectively. No fake modulation is seen in the angular distribution. This is a practical advantage of the geometrical symmetry of GAP's configuration, as shown in figure 3.

In figure 7, we show the light curves with the plastic–CsI coincidence events, corrected for each angular phase in the

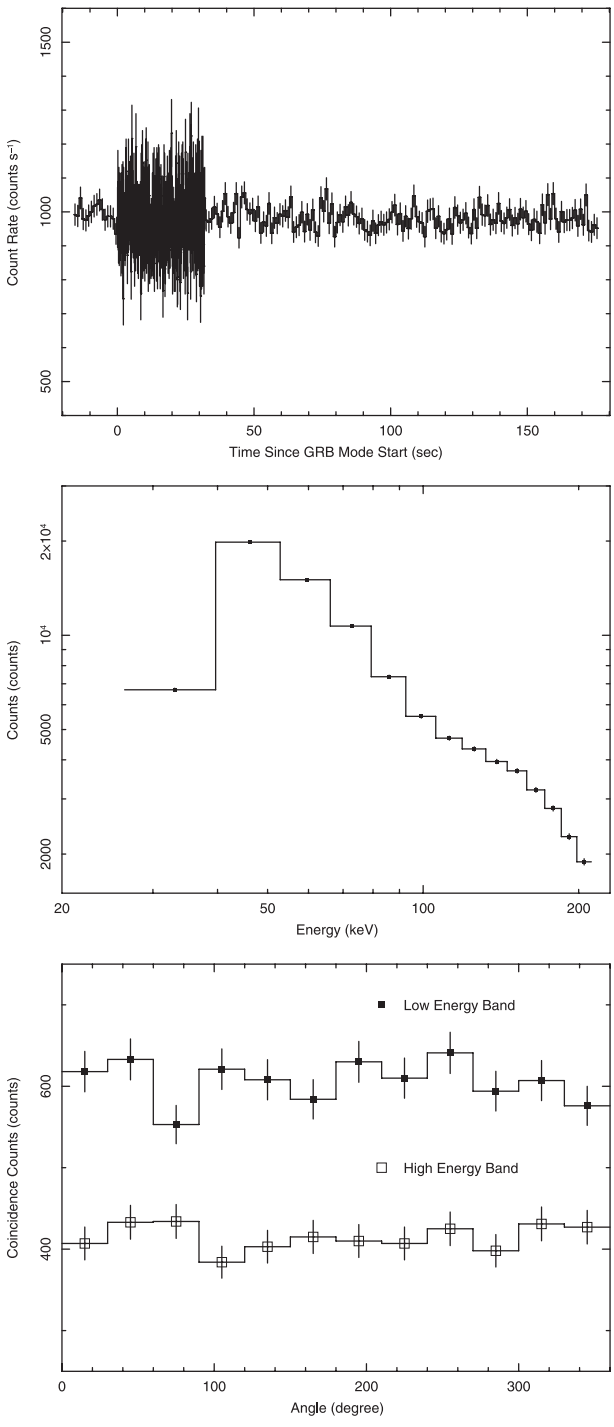

Fig. 6. Data examples of the GRB mode, obtained by sending the manual GRB-mode command in the orbit. These data are equivalent to the cosmic X-ray/gamma-ray background. Top: Light curve of gamma-ray events in the range of between LD and UD of each sensor. The time resolution for the first 32 s from the trigger time ($t = 0$) is 125 ms, so the error bars accompanying the data become large. Middle: The background spectrum sum of 12 CsI sensors in the time range of from $t = 0$ to $t = 176$ s in 16 PHA channels. Bottom: The polarization data of the low-energy (filled square) and high-energy (open square) bands in the interval of time between $t = -16$ s and $t = 176$ s.

Table 1. Time resolution of the GRB mode.

Time [s]	Light curve (LD–UD)	Polarization (low:LD–HITPAT_LH) (high:HITPAT_LH–UD)	Spectrum (LD–UD) (16 channels)
$-16 \leq T < 0$	1 s	1 s	N/A
$0 \leq T < 32$	125 ms	1 s	—
$32 \leq T < 176$	1 s	1 s	—
$0 \leq T < 176$	—	—	176

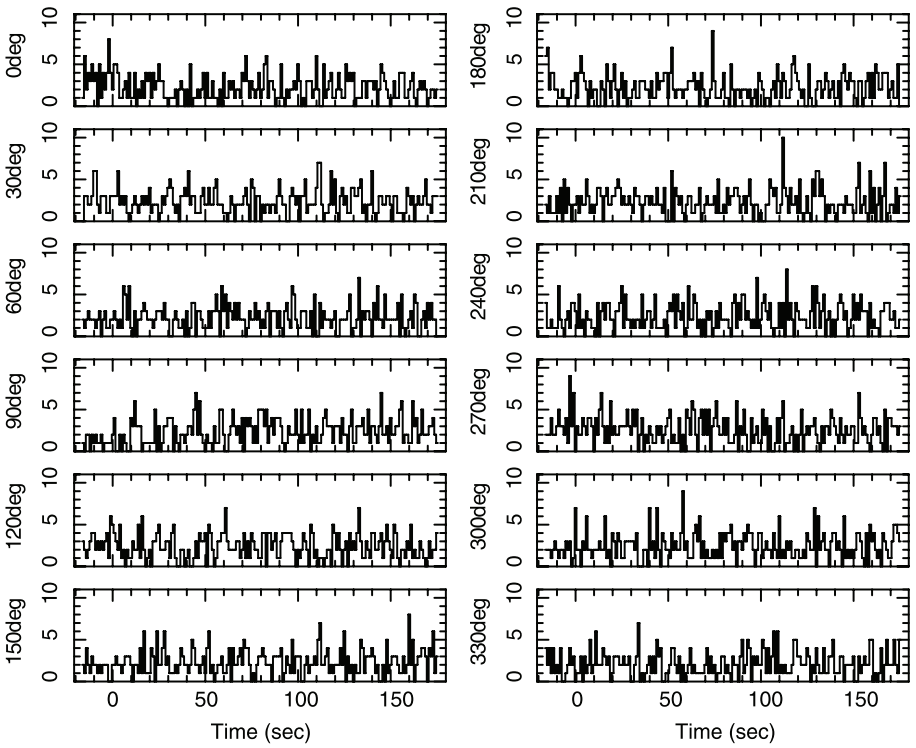

Fig. 7. Polarization (hit-pattern) light curves with a time resolution of 1 s, obtained by the manual GRB mode. The time $t = 0$ denotes the GRB trigger time. GAP always monitors the rotation period of IKAROS, so this light curve has already been corrected for its rotation phase every 125 ms. We can obtain these 12 sets of polarization data in two energy bands.

manual GRB mode. Here, we determined the phase angle $\phi = 0$ as the CsI No.1 when the Sun pulse signal comes from the spacecraft. When GAP enters the GRB mode, it starts measuring the polarization (hit-pattern of plastic–CsI) every second to provide time-resolved data. Therefore, we are able to obtain time resolved polarization data. GAP always monitors the rotation period of IKAROS, so this polarization light curve has already been corrected for its rotation phase every 125 ms. The polarization is measured in the two energy bands, denoted High and Low. The energy range of the low-energy polarization is equivalent to that of between LD and HITPAT_LH. Similarly, the high-energy polarization is measured in the range of from HITPAT_LH to UD. Here, HITPAT_LH is the boundary channel of energy divided into the low- and high-energy bands, and we can change HITPAT_LH by command. The nominal value of HITPAT_LH is set for ~ 100 keV.

When the GRB trigger is set, the GAP-CPU latches the GRB trigger time (clock counter), and stores it in the SRAM. GAP also records the Sun pulse time (phase) of the trigger time and the rotation period of the IKAROS spacecraft at that time. Therefore, we can determine the phase angle of the polarization vector around the IKAROS rotation axis. GAP also stores total photon counts of each phase angle (30° angular resolution) during the period of the GRB mode, so we have the possibility of determining very rough directions of bright GRBs.

3.3. Calibration Mode and Onboard Calibration

We mounted seven weak radio isotope sources of ^{241}Am on the top panel of GAP, one for two CsI scintillators and one for the plastic at the center. The count rate of ^{241}Am is ~ 10 Hz per CsI. In the calibration mode, we obtained the detailed spectra in 64 energy channels for each sensor. Therefore, we can measure the pulse height of the 59.5 keV line of ^{241}Am with high precision. These spectral data contain only the single-hit

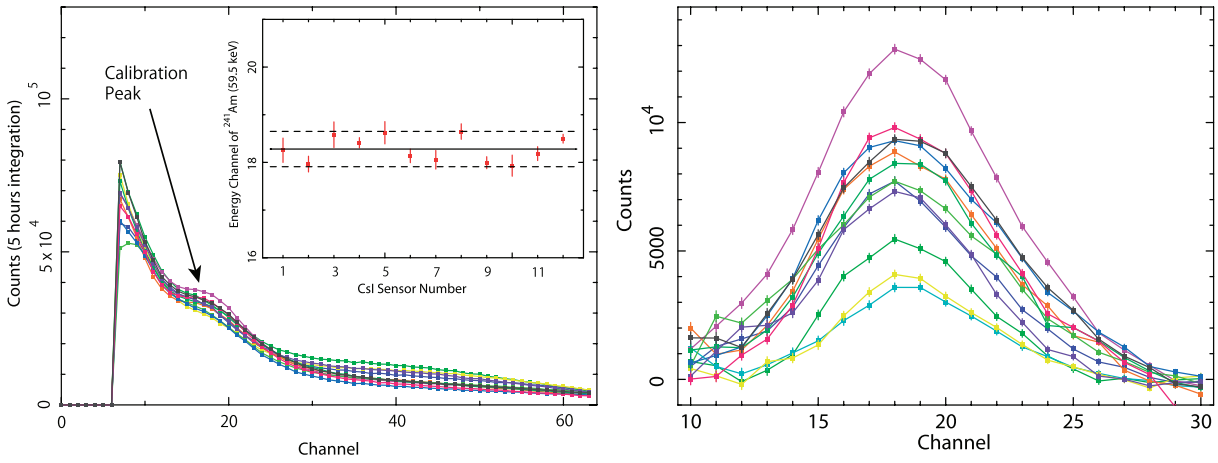

Fig. 8. Left: Onboard calibration spectra of 12 CsI scintillators with ^{241}Am (59.5 keV) peak. All spectra show low-energy cut at around 23 keV with the LD. The panel inserted on the figure shows the ^{241}Am peak channel of 12 CsI scintillators. The solid line is the weighted average, and two dashed lines show the boundaries of $\pm$ 2% deviations. We succeeded in adjusting all PMT gains within the 2% level. Right: Residuals of calibration spectra with the flux of the ^{241}Am line set for zero, but with the continuum parameters at their best-fit values.

photon events because the coincidence events, e.g., plastic–CsI and CsI–CsI, lose some of the energy, and it is lower than 59.5 keV. Since the integration time can be chosen in the range of from 30 s to 4.3 hr in steps of 2 min, we can flexibly count up photons in the environment with any background rate, and avoid buffer overflow.

In figure 8, we show 12 CsI spectra obtained in orbit. These spectra are equivalent to 5 hr integration after careful gain adjustments. The 59.5 keV line of ^{241}Am is clearly observed. The inserted panel in figure 8 shows the uniformity of the peak energy channel of the calibration line for each CsI sensor. The best fit line is the 18.2 channel, and two dashed lines show the upper and lower boundaries of $\pm$ 2% deviations from the best fit. This demonstrates that the 12 CsI gains have been adjusted to within an error of 2%.

We have tested whether the gain is affected by the counting rates, which is important when GAP detects intense GRBs. Using test pulses, we confirmed that the gains of all sensors did not change at 50 kHz at least. This counting rate is higher by one order of magnitude than one of the brightest GRBs expected from the BATSE catalog. Moreover, we also confirmed that all gains of CsI sensors have the same trend as a function of the temperature. IKAROS is an interplanetary spacecraft, so the temperature of spacecraft body and GAP, itself, changes quite slowly. Therefore, we can say that the gains of all sensors are stable and well ordered. We, of course, monitored these gains once every two or three weeks, and confirmed that they were quite stable within the $\pm$ 2% deviations during the first two months.

4. Detector Capability Estimated by Geant-4 Simulation

In this section, we describe Monte Carlo simulations with the Geant-4 simulator to estimate the capability of GAP, and verify the model parameters. We first show that the Geant-4 simulation is consistent with an idealized experiment with a high-polarized monochromatic X-ray beam at the KEK (High Energy Accelerator Research Organization) photon factory.

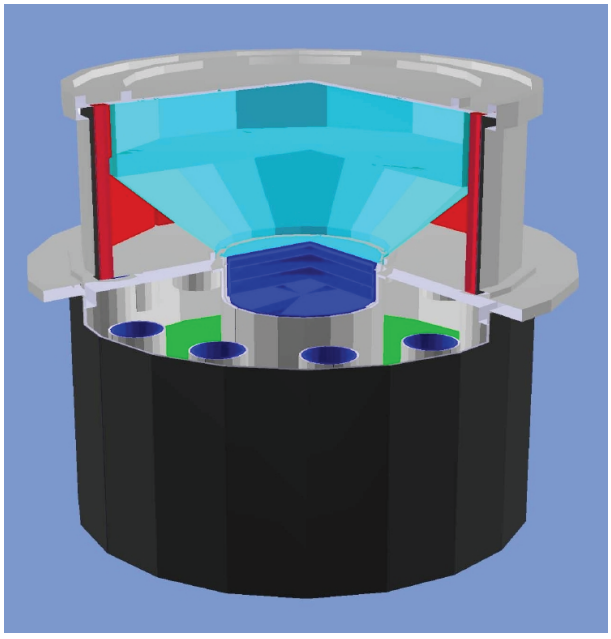

Fig. 9. Geometrical mass model of GAP for the Geant-4 simulator. Scintillators (plastic: light blue; CsI: red), PMTs (blue), chassis case (aluminum: light gray; lead shields: dark gray), electronics circuits, and high-voltage modules (green) with appropriate mass elements.

After that, we introduce the basic parameters of an X-ray and gamma-ray polarimeter: a modulation factor, a detection efficiency of polarized gamma-ray, a minimum detectable polarization, and some examples of the detector response for diagonal incident photons. We need more experiments and investigations for a detailed discussion about the in-flight performance of GAP when compared with the Geant-4 simulation. Therefore, in this section, we show only the fundamental detector capability without any background on the purpose of ready comparison with the other detectors.

As shown in figure 9, we set a Geant-4 model of geometries

and mass of elements, which represent the real detector as precisely as possible. The cylindrical aluminum cases of the detectors (light gray) are covered by thin lead sheets (dark gray), except for the top panel window, so as to avoid any scattered photons from the spacecraft body. Thus, direct X-rays from the top direction illuminate the plastic, and also the edge of the CsI. The plastic and 12 CsI scintillators are shown in light blue and in red, respectively. The 13 PMTs are shown in blue, and all of them are covered with thin aluminum cylinders. The green sheet inside the detector case represents three layers of electric circuits. Two high-voltage modules are also modeled while they are behind the detector case. Additionally, we consider a simplified spacecraft body with thick aluminum sheets (mass equivalent) as a scatterer in the geometry model (not shown in figure 9). The outputs from this simulator are edited in the same types of data as GAP accumulates. Moreover, to investigate physical interaction between the incident gamma-ray photons and GAP, we also output more detailed information, such as the spectrum of each sensor, the coincidence spectrum of each sensor, and polarization information for single as well as double and multiple coincidence, while GAP cannot distinguish the multiple scattering in the central plastic.

4.1. *Modulation Factor, Efficiency, and Pre-Flight Calibration*

The modulation factor (M_{100}) is one of the most important parameters to describe the detector sensitivity for polarization measurements. The definition of the M_{100} is the ratio of the amplitude of modulation to the average level of the modulation curve of the detector response to 100% polarized gamma-rays. According to the cross section of the Compton effect in equations (1) and (3), the angular distribution of the scattering photon basically shows $\sin^2\phi$ modulation. Figure 10 shows the simulated modulation curves when we assume the condition that the gamma-ray photons with 100% polarization (filled square) and nonpolarization (open square) irradiate the front of GAP. The GAP's modulation factor, M_{100}, is estimated by the Geant-4 simulator as

$$M_{100} \equiv \frac{N_{\max} - N_{\min}}{N_{\max} + N_{\min}} = \frac{\text{amplitude of modulation}}{\text{average of modulation}}. \quad (4)$$

Here, $N_{\max}$ and $N_{\min}$ are the maximum and minimum counts of the angular distribution of 100% polarized scattered photons.

4.2. *Ground-Based Calibration at KEK Photon Factory*

To verify the mass model and to confirm the Geant-4 simulation, we carried out ground-based calibration using the Proto-Flight Model (PFM-GAP) before the launch. The Flight Model (FM-GAP) was not ready to use at that time, so we used the PFM-GAP for a test on 2008 November 1–5 at KEK photon factory (beam line PF-14A). The only difference between FM-GAP and PFM-GAP is the thickness of the central plastic and the height of CsI. The PFM-GAP is 7 cm in thickness and height, but we changed the design of FM-GAP to 6 cm to reduce the weight of the FM system.

We tested a very limited number of parameters, such as the modulation factor (MF) and also the detection efficiency (η).

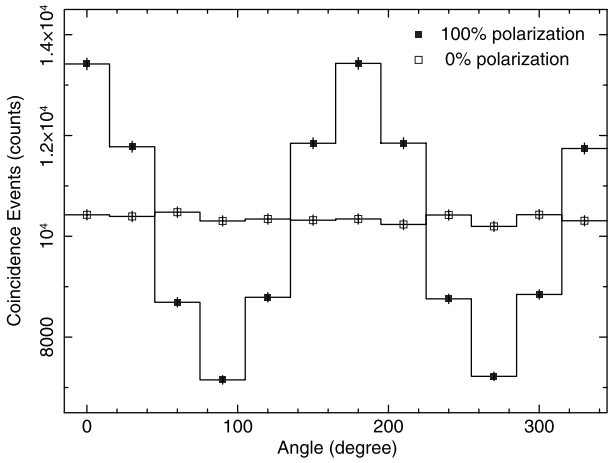

Fig. 10. Example of the modulation curve for monochromatic gamma-ray of 100 keV with 100% polarization (filled square) and nonpolarization (open square). For nonpolarized gamma-rays, the modulation curve becomes constant and its deviation is under 1%.

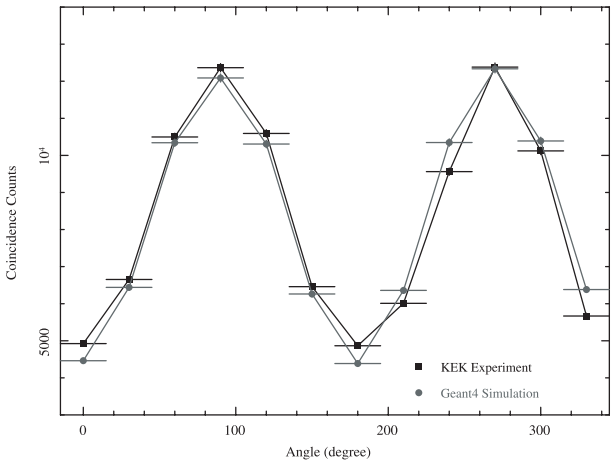

Fig. 11. Modulation curves for the monochromatic 80 keV with the 82% polarized X-ray beam measured by the experiment at KEK photon factory (black filled square), and the result by the Geant-4 simulation for the PFM-GAP model in the same condition (dark gray filled circle). Both modulation curves are in close agreement with each other, and this fact strongly supports the validity of the mass model for PFM-GAP in Geant-4. The same mass model is used for the FM-GAP except for the thickness of plastic.

A monochromatic 80 keV pencil beam of 0.8 mm in diameter with 82% polarization irradiated the center of PFM, i.e., only the center of plastic scintillator. The beam is so narrow that we could not carry out uniform irradiation of the top surface. The observed distribution of coincident photons in the 12 CsI units is shown in figure 11 together with the Geant-4 simulation for the mass model. The black filled square and dark gray filled circle are the result of the KEK experiment and those of the Geant-4 simulation by the experiment beam, respectively. Both curves agree well, which strongly supports the validity of the Geant-4 mass model for the PFM-GAP detector. The modulation factor for the 82% polarized beam at the center position is $MF = 0.43$ by the experiment, which is equivalent to

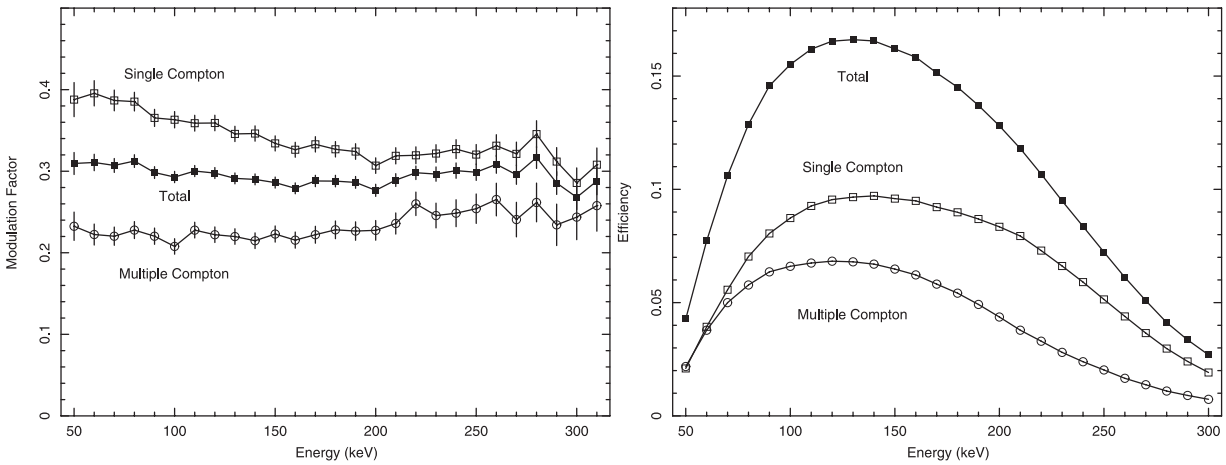

Fig. 12. Modulation factor (left) and the efficiency of polarization measurement (right) of FM-GAP as a function of the incoming gamma-ray energy calculated by the Geant-4 simulation. Here, the modulation factor is determined by equation (4). The open square and circle indicate the single and multiple scattering events in the central plastic, respectively. The filled square is the total performance of FM-GAP. The modulation factor is rather flat in the range of between 50–300 keV, while the efficiency is optimized around the energy of 100–150 keV.

$M_{100} = 0.52$ to the 100% polarized beam. We emphasize that this modulation factor of $M_{100} = 0.52$ is for the pencil beam experiment irradiating only the GAP center (not the entire surface of GAP).

In figure 12 (left and right panels), we show the modulation factor and efficiency, which were calculated for the mass model of FM-GAP using the same logics of the PFM, as a function of the photon energy for the case of uniformly irradiating the full surface of FM-GAP. Each panel shows three curves of the modulation factor and the efficiency for single and multiple Compton-scattering events in the central plastic, and also for the total event. Of course, GAP cannot resolve multiple scattering in the plastic, but we introduce the detector capability, including multiple scattering effects for the modulation factor and efficiency. The total modulation factor for the FM-GAP is rather flat as $M_{100} = 0.30$ in the range of between 50–300 keV. In the case of uniform irradiation of the top surface, this value is lower than that in the KEK pencil beam experiment ($M_{100} = 0.52$). The efficiency (η), which is defined as the ratio of the number of plastic–CsI coincidence events to the total incoming photons, is ~ 0.16–0.17 at around 100–150 keV. As shown in figure 12 (left), the multiple scattering event in the plastic reduces the modulation factor, but it is not so crucial. The efficiency of single scattering dominates that of multiple scattering in all energy bands. Since the depth and diameter of the plastic scintillator are optimized as 1 Compton length for 100 keV photon, the efficiency in the energy below 100 keV is suppressed by self-absorption in the plastic. Although the value of the modulation factor at the low energy is also strongly influenced by the setting of LD and the energy resolution (ΔE), we included these effects in the Geant-4 simulations as LD = 7 keV and $\Delta E = 0.21/\sqrt{E/(60\,\mathrm{keV})}$ for the plastic scintillator and LD = 30 keV and $\Delta E = 0.16/\sqrt{E/(60\,\mathrm{keV})}$ for the CsI ones.

4.3. Minimum Detectable Polarization

Using the modulation factor (M_{100}) and the efficiency shown in figure 12, we estimated the rate of GRBs whose polarization is detected. We used the definition of minimum detectable polarization (*MDP*) as the sensitivity for the polarization measurement (e.g., Weisskopf et al. 2010). The minimum detectable polarization is defined as

$$MDP = \frac{n_\sigma}{M_{100}} \frac{\sqrt{(FS\eta + B)T}}{FS\eta T}, \quad \text{where} \tag{5}$$

F, GRB photon flux (counts cm^{-2} s^{-1});

B, coincidence background count rate (counts s^{-1});

S, geometrical area (cm^2);

T, GRB duration (s).

Here, n_σ is the significance of detection. If we assume the 99% confidence level, $n_\sigma = 3\sqrt{2}$ (Weisskopf et al. 2010).

The detectability of polarization depends on the source flux (F), the total duration (T), and the coincidence background count rate (B); that is, the total number of photons in the modulation curve. We assume that the main background component for the plastic–CsI coincidence event is the CXB. The cosmic rays are removed with the upper-discriminator, and the activation of CsI is negligible when compared with the CXB flux, because the net volume of CsI is very small. We measured B as a few counts s^{-1} for each CsI scintillator, whose value is consistent with the rate calculated from the CXB spectrum reported by Gruber et al. (1999). Then, using the Compton Gamma-Ray Observatory (CGRO)-BATSE catalog, which contains 2135 GRB samples, we calculated *MDP* for each event. We converted the energy fluence in the range of 50–300 keV, which almost matches the energy coverage of GAP, into the photon flux (F) with an average power-law index of $\alpha = -1$ (Preece et al. 2000). We used T_{90} listed in the BATSE catalog as the total duration (T), where T_{90} is measured as the time duration covering 90% of the total observed photons. If we assume that the degree of polarization of GRBs is $\sim 40\%$ (Lazzati et al. 2004; Toma et al. 2009), we can expect to detect polarization with a rate of 2–4 GRBs/yr within the solid angle of the incident direction of $\theta < 30^\circ$. These are approximately

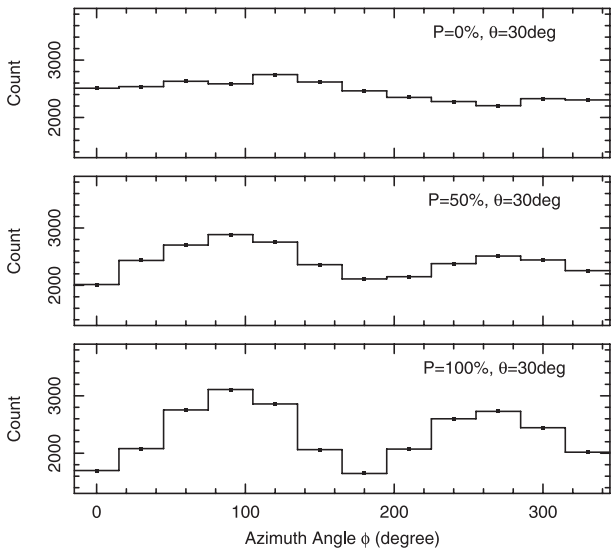

Fig. 13. Examples of simulated modulation curve by Geant-4 for the angle of incident photon as $\theta = 30°$, and the azimuth angle of $\phi = 90°$. The top, middle, and bottom panels show the modulation curves of polarization degrees of $P = 0\%$, 50%, and 100%, respectively, in the case of the power-law spectrum with a photon index of -1. We assumed the polarization vector to be parallel to the detector surface in these simulations.

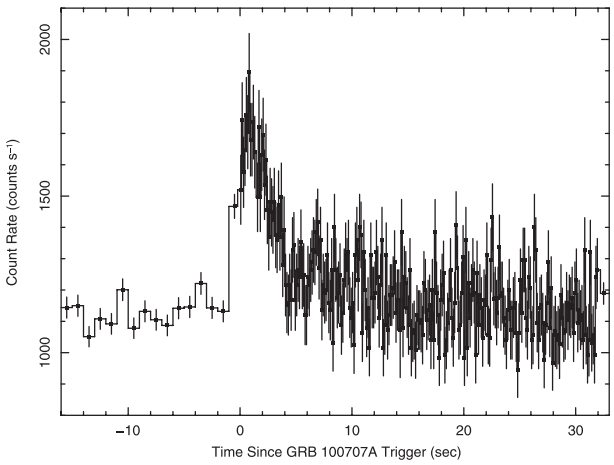

Fig. 14. Lightcurve of GRB 100707A detected by IKAROS-GAP. This event occurs at $\theta = 90°$ measured from the GAP detector axis.

10% of the brightest events in the CGRO-BATSE catalog. In this estimation, we used $M = 0.25$ and $\eta = 0.15$, which are smaller than the values shown in figure 12, but roughly consistent with the results for incident angles of 20°–30°, instead of random incident angles for each event.

4.4. Response for Polarized Beam of Diagonal Incident Photon

In figure 13, we show the detector response simulated by the Geant-4 for the incident photons from the diagonal direction. We assume an incident direction of $\theta = 30°$ from the detector axis of GAP, and an azimuth angle of $\phi = 90°$. The top, middle, and bottom panels show the response of polarization degrees of $P = 0\%$, 50%, and 100%, respectively. We assume that the polarization vector is parallel to the detector surface in these simulations.

In the case of $P = 0\%$, the modulation curve basically depends on $\sin\phi$. This is because the GAP surface has an elliptic shape, as viewed from the diagonal position. On the other hand, the modulation curve of polarized gamma-rays shows the composition of $\sin^2\phi$ [see equation (3)] and $\sin\phi$ based on the response for the diagonal incident photons. As shown in the middle and bottom panels of figure 13, the modulation with two peaks will be observed for polarized gamma-rays, but the peak intensities are different from each other by the diagonal effect. The position of the peak is also influenced by the vector of the incident polarization.

5. First Detection of GRB

Since the switch-on on 2010 June 21, GAP detected GRB 100707A on 2010 July 7. The light curve is shown in figure 14. The trigger time was $T_0 =$ 00:47:22.878 UT with an uncertainty of ± 0.250 s at a distance of 17917783 km from Earth. The direction of IKAROS from Earth on July 7 was $(\alpha, \delta) = (209.^\circ71, -24.^\circ32)$. The time accuracy will be improved to ± 0.125 s in the near future after careful calibration of the clock system. This burst was also triggered by Fermi-GBM, Suzaku-WAM, Konus-Wind, and Messenger-GRN. Therefore, the direction of GRB 100707A was determined by the interplanetary network (IPN). The error box of the GRB direction by the IPN was found to be $(\alpha, \delta) = (358.^\circ02^{+0.^\circ75}_{-0.^\circ90}, -8.^\circ66^{+3.^\circ36}_{-3.^\circ00})$ by Hurley et al. (2010).

We checked the consistency between our clock system and the reported IPN GRB direction. By cross-correlating the lightcurves between the IKAROS-GAP and Suzaku-WAM, the difference in the arrival time of maximum photon flux between GAP and WAM is $\Delta T = 42.230 \pm 0.250$ s. Then, the GRB position was calculated as the cone angle of $\theta_{\rm GAP} = 43.^\circ68 \pm 0.^\circ36$, measured from the axis between IKAROS and Earth. Here, we assumed that the error of angle is due to the time accuracy (0.250 s) of the GAP system. The GAP cone is consistent with the GRB position reported by Hurley et al. (2010). Therefore, we conclude that GAP can join the IPN system, which consists of such components as Fermi, Konus-Wind, and Messenger-GRN.

According to the IKAROS attitude, the axis of the GAP direction was $(\alpha, \delta) = (265.^\circ257, -18.^\circ337)$ on 2010 July 7. Therefore, the incident direction of GRB 100707A is almost $\theta = 90°$ from the center of GAP field of view. In this case, most of the incident gamma-ray photons were absorbed by the surrounding CsI scintillators, and did not reach the plastic, and the photon statistics of the coincidence event become poor. Therefore, it is quite difficult to perform polarization analysis of this event. According to the Konus-Wind results, the peak energy is $E_{\rm p} = 264^{+49}_{-40}$ keV (Golenetskii et al. 2010), and Fermi-LAT also detected this event (Pelassa et al. 2010); GRB 100707A was thus a hard and bright burst. This hard spectrum could enable GAP to detect this event even if the side cylinder and the bottom are shielded by thin lead.

6. Summaries

1. We developed a gamma-ray burst polarimeter, "GAP", aboard the small solar power sail demonstrator IKAROS.
2. The IKAROS spacecraft was launched on 2010 May 21, We performed calibrations since the switch-on of 2010 June 21, and succeeded in setting all CsI gains within 2%. After that we started GRB observations.
3. Because the geometrical shape of GAP is highly symmetrical, the systematic uncertainty due to spurious (fake) modulation is quite low for the CXB. Actually, we have demonstrated the flatness of the modulation curve with the 1% level obtained by the CRAB mode data in subsection 3.1 and figure 5 (bottom). However, we should consider the systematic uncertainty caused by the incident gamma-rays from off-axis directions when we analyze the GRB polarization. Since this systematic uncertainty may depend on the incident angle, we have to estimate it with the PFM-GAP event by event.
4. The pre-flight calibration at KEK and the Geant-4 simulation are fully consistent and strongly support the validity of our detector. GAP measures the angular anisotropy of Compton scattering with real coincidence events between the plastic and 12 CsI scintillators. These two points are advantageous to gamma-ray polarimetry, and will be the basis for polarimetric observations of normally incident GRBs, other impulsive events (e.g., magnetar flares), and possibly hard X-ray pulsars.
5. According to the current operation, the detection rate of GRBs is about once a week. For bright events, we can discuss the polarization degree. The expectation is to detect polarization from 2–4 events per year if GRBs show $\sim 40\%$ polarization as theoretically predicted.
6. GAP will observe gamma-ray polarization in the entire field of view with the CRAB mode. We will measure the degree of polarization of the Crab Nebula due to the lack of any other bright source in the vicinity, in quiescence. Of course, we cannot separate the contributions from individual objects. However, the Crab Nebula is located at the opposite direction of the Galactic center, and there are few bright objects close to the Crab Nebula. Thus, we may be able to perform polarization analysis for the Crab Nebula.
7. We will utilize the IPN-derived position for detected GRBs in GAP analyses, and will provide GRB trigger times to the IPN as a member of the network.

We deeply thank the operation staff members at the Tokyo Metropolitan Industrial Technology Research Institute and Dr. Satoshi Hatori, Dr. Kyo Kume, and technical staff at the Wakasa-Wan Energy Research Center for their assistances during the qualification tests of electrical devices. We also thank Mr. Takano at the Industrial Research Institute of Ishikawa for his support during the period of mechanical tests. We are grateful to Professor R. E. Rothschild for a detailed reading, and useful comments to this paper as a referee. This work is supported in part by Grants-in-Aid from the Ministry of Education, Culture, Sports, Science and Technology (MEXT) of Japan, No. 20674002 (DY) and No. 18684007 (DY), and also this is supported by the Steering Committee for Space Science at ISAS/JAXA of Japan (TM).

References

Amati, L. 2006, MNRAS, 372, 233
Amati, L., et al. 2002, A&A, 390, 81
Bellazzini, R., et al. 2003, Proc. SPIE, 4843, 383
Coburn, W., & Boggs, S. E. 2003, Nature, 423, 415
Costa, E., et al. 1997, Nature, 387, 783
Dean, A. J., et al. 2008, Science, 321, 1183
Fenimore, E. E., & Ramirez-Ruiz, E. 2000, astro-ph/0004176
Frail, D. A., et al. 2001, ApJ, 562, L55
Galama, T. J., et al. 1998, Nature, 395, 670
Ghirlanda, G., Ghisellini, G., & Lazzati, D. 2004, ApJ, 616, 331
Golenetskii, S., et al. 2010, GCN Circ., 10948
Gruber, D. E., Matteson, J. L., Peterson, L. E., & Jung, G. V. 1999, ApJ, 520, 124
Gunji, S., et al. 2007, Proc. SPIE, 6686, 18
Gunji, S., Kudo, E., & Sakurai, H. 1997, IEEE Nucl. Sci. Symp. Conf. Rec., 610
Gunji, S., Sakurai, H., Noma, M., Takase, E., Sato, T., & Misawa, H. 1994, IEEE Trans. Nucl. Sci., 41, 1309
Hjorth, J., et al. 2003, Nature, 423, 847
Hurley, K., et al. 2010, GCN Circ., 10947
Kamae, T., et al. 2008, Astroparticle Phys., 30, 72
Kawaguchi, J., Mori, O., Tsuda, Y., Yamamoto, T., Funase, R., Sawada, H., Kawakatsu, Y., & Morimoto, M. 2008, Proc. 59th Int. Astronaut. Congr. (Reston, VA: AIAA), IAC-08.A3.6.15
Kestenbaum, H. L., Cohen, G. G., Long, K. S., Novick, R., Silver, E. H., Weisskopf, M. C., & Wolff, R. S. 1976, ApJ, 210, 805
Kishimoto, Y., et al. 2007, IEEE Trans. Nucl. Sci., 54, 561
Kitamoto, S., et al. 2010, Rev. Sci. Instrum., 81, 023105
Lamb, D. Q., et al. 2004, New Astron. Rev., 48, 423
Lazzati, D., Rossi, E., Ghisellini, G., & Rees, M. J. 2004, MNRAS, 347, L1
McGlynn, S., et al. 2007, A&A, 446, 895
Mihara, T., & Miyamoto, H. 2004, Proc. X-ray Polarimetry Workshop (Menlo Park, CA: SLAC)[2]
Mori, O., et al. 2009, Trans. Jpn. Soc. Aeronaut. and Space Sci., Space Technol. Jpn., Vol.7, No.ists26, Pd87
Murakami, T., Yonetoku, D., Sakashita, T., Morihara, Y., Kikuchi, Y., Gunji, S., Tokairin, N., & Mihara, T. 2010, in AIP Conf. Proc., 1279, Deciphering the Ancient Universe with Gamma-Ray Bursts, ed. N. Kawai & S. Nagataki (New York: AIP), 227
Norris, J. P., Marani, G. F., & Bonnell, J. T. 2000, ApJ, 534, 248

[2] ⟨http://www-conf.slac.stanford.edu/xray_polar/X-Ray%20presentations/SLACmihara.pdf⟩.

Nousek, J. A., et al. 2006, ApJ, 642, 389
Panaitescu, A., & Kumar, P. 2001, ApJ, 560, L49
Pelassa, V., & Pesce-Rollins, M. 2010, GCN Circ., 10945
Piran, T. 1999, Phys. Rep., 314, 575
Preece, R. D., Briggs, M. S., Mallozzi, R. S., Pendleton, G. N., & Paciesas, W. S. 2000, ApJS, 126, 19
Rees, M. J., & Mészáros, P. 1992, MNRAS, 258, L41
Rutledge, R. E., & Fox, D. B. 2004, MNRAS, 350, 1288
Sakamoto, T., et al. 2004, ApJ, 602, 875
Salvaterra, R., et al. 2009, Nature, 461, 1258
Schaefer, B. E., Deng, M., & Band, D. L. 2001, ApJ, 563, L123
Suzuki, T., et al. 2006, Jpn. J. Appl. Phys., 45, 274
Swank, J., Kallman, T., & Jahoda, K. 2008, 37th COSPAR Sci. Assem., 3102
Tamagawa, T., et al. 2006, Proc. SPIE, 6266, 62663W
Tanimori, T., Kubo, H., Miuchi, K., Nagayoshi, T., Orito, R., Takada, A., Takeda, A., & Ueno, M. 2004, New Astron. Rev., 48, 263
Tanvir, N. R., et al. 2009, Nature, 461, 1254
Toma, K., et al. 2009, ApJ, 698, 1042
Waxman, E., Kulkarni, S. R., & Frail, D. A. 1998, ApJ, 497, 288
Weisskopf, M. C., Cohen, G. G., Kestenbaum, H. L., Long, K. S., Novick, R., & Wolff, R. S. 1976, ApJ, 208, L125
Weisskopf, M. C., Elsner, R. F., & O'Dell, S. L. 2010, Proc. SPIE, 7732, 77320E
Wigger, C., Hajdas, W., Arzner, K., Güdel, M., & Zehnder, A. 2004, ApJ, 613, 1088
Yonetoku, D., et al. 2010, in Proc. X-ray Polarimetory, ed. R. Bellazzini et al. (New York: Cambridge Univ. Press), 339
Yonetoku, D., Murakami, T., Masui, H., Kodaira, H., Aoyama, Y., Gunji, S., Tokanai, F., & Mihara, T. 2006, Proc. SPIE, 6266, 6266C
Yonetoku, D., Murakami, T., Nakamura, T., Yamazaki, R., Inoue, A. K., & Ioka, K. 2004, ApJ, 609, 935